Modeling the activity of short-term slow slip events along deep subduction interfaces beneath Shikoku, southwest Japan

Bunichiro Shibazaki,[1] Shuhui Bu,[2] Takanori Matsuzawa,[3] and Hitoshi Hirose[3]

[1] We developed a model of short-term slow slip events (SSEs) on the 3-D subduction interface beneath Shikoku, southwest Japan, considering a rate- and state-dependent friction law with a small cutoff velocity for the evolution effect. We assume low effective normal stress and small critical displacement at the SSE zone. On the basis of the hypocentral distribution of low-frequency tremors, we set three SSE generation segments: a large segment beneath western Shikoku and two smaller segments beneath central and eastern Shikoku. Using this model, we reproduce events beneath western Shikoku with longer lengths in the along-strike direction and with longer recurrence times compared with events beneath central and eastern Shikoku. The numerical results are consistent with observations in that the events at longer segments have longer recurrence intervals. The activity of SSEs is determined by nonuniform frictional properties at the transition zone. We also attempt to model the very low frequency (VLF) earthquakes that accompany short-term SSEs, on a 2-D thrust fault. We consider a local patch in which the friction parameters are varied. In the case that critical displacement is very small at the patch, fast multiple slips occur at the patch. In the case that the effective normal stress is high at the patch, the patch acts as a barrier to SSEs; when it ruptures, however, rapid slip occurs. Because the source time functions of these cases are somewhat different, it would be possible in the future to assess if either case is an appropriate model for VLF earthquakes.

1. Introduction

[2] Recent high-resolution observations of crustal movements have revealed the occurrence of slow slip events (SSEs) along the deeper parts of seismogenic faults. Two types of SSEs have been observed: long-term SSEs with durations of several months to several years and short-term SSEs with durations of several days to several weeks. In general, long- and short-term SSEs have long and short recurrence intervals, respectively; consequently, it would be appropriate to refer to these events as long- and short-interval SSEs, respectively.

[3] One example of long-term SSEs is events that occur at the deep subduction interface beneath the Bungo Channel in the western part of the Nankai Trough, Japan [*Hirose et al.*, 1999; *Ozawa et al.*, 2001; *Hirose and Obara*, 2005], with a duration of several months and recurrence interval of approximately 6 years. *Ozawa et al.* [2002] detected a long-term SSE in the Tokai region, a well-known seismic gap along

the Suruga-Nankai Trough. The event started in March 2001 and continued until the spring of 2006.

[4] Other studies have reported the occurrence of short-term SSEs with a duration of several days to weeks. For example, a silent slip of about 2 cm with a several weeks was detected over an area of 50×300 km^2 on the deeper Cascadia subduction interface [*Dragert et al.*, 2001]; the recurrence interval of these SSEs is 14 months [*Miller et al.*, 2002; *Dragert et al.*, 2004]. *Obara* [2002] reported nonvolcanic low-frequency tremors (LFTs) in a subduction zone in southwest Japan. *Rogers and Dragert* [2003] found that SSEs upon the deeper Cascadia subduction interface are accompanied by LFTs similar to those reported in the southwest Japan subduction zone. Based on tiltmeter observations, *Obara et al.* [2004] and *Hirose and Obara* [2005] also found that short-term SSEs with a duration of several days occur in association LFT activity in the southwest Japan subduction zone; the recurrence intervals of these SSEs are 3-6 months.

[5] Recently, *Ito et al.* [2007] found that very low frequency (VLF) earthquakes are accompanied by and migrate with the activity of LFTs and short-term SSEs. The magnitudes of these VLF earthquakes are M 3.1–3.5, considerably smaller than the magnitudes of short-term SSEs. Ito et al. proposed a scenario for the occurrence of these VLF earthquakes, in which stronger coupled patches of VLF earthquakes are surrounded by a region of short-term SSEs. At

[1]International Institute of Seismology and Earthquake Engineering, Building Research Institute, Tsukuba, Japan.
[2]Department of Computer Science, University of Tsukuba, Tsukuba, Japan.
[3]National Research Institute for Earth Science and Disaster Prevention, Tsukuba, Japan.

the propagation front of a short-term SSE, the shear stress increases at the patches of VLF earthquakes; these patches eventually rupture at a high slip velocity once the shear stress reaches the critical stress value. *Ide et al.* [2007] determined a general scaling law for slow events from LFTs to VLF earthquakes and SSEs. In their scaling, seismic moment increases linearly with time. This scaling law suggests that the characteristic propagation velocity increases with decreasing event size. *Shelly et al.* [2007] also found that LFT activity does not evolve in a smooth and steady fashion; instead, it involves numerous rapid migrations over a small distance and for a short duration, with a speed of 25–150 km/h along the dip direction. They suggested that slip failure occur repeatedly at the stronger patches during the continuous slip in the surrounding regions of the fault.

[6] To clarify the generation process of SSEs, it is necessary to understand the environmental characteristics of the generation zone. *Dragert et al.* [2004] proposed a model for plate motion and stress accumulation across the Cascadia subduction interface, in which short-term SSEs extend the transition zone from the 350°C isotherm to the 550°C isotherm. Based on the estimated temperature distribution within the western Japan subduction zone [*Yoshioka and Murakami*, 2007], the temperature at the location of short-term SSEs is inferred to lie in the range from 400 to 500°C. Therefore, it is necessary to consider the frictional properties of the unstable-stable transition zone to successfully model short-term SSEs. As indicated by *Dragert et al.* [2004], LFTs and short-term SSEs in southwest Japan occur along the lower limit of the coseismic rupture area estimated by *Sagiya and Thatcher* [1999] for the 1944 Tonakai and 1946 Nankaido earthquakes. Therefore, when the main event occurs in the seismogenic region, rapid rupture does not propagate into the region of short-term SSEs.

[7] Recent studies have suggested that pore fluid pressure is very high at deep subduction interfaces in western Japan. Based on seismological studies, *Kodaira et al.* [2004] identified a highly reflective zone with a high Poisson's ratio in the deeper extension of the Tokai segment of the Nankai Trough. Kodaira et al. suggested that the high pore fluid pressure within these zones leads to the occurrence of long-term SSEs. *Shelly et al.* [2006] revealed that low-frequency earthquakes occur on the plate interface, which suggest that all LFT activity also occurs on the plate interface, coincident with the inferred zone of slow slip. The generation zone of low-frequency earthquakes corresponds to the area of high v_p/v_s. Their results also suggest that the high pore fluid pressure enhances the generation of short-term SSEs. *Kamaya and Katsumata* [2004] considered the mechanisms of LFTs in western Japan using phase diagrams for representative materials found in and around the descending slab. They suggested that these LFTs are caused by water released by the dehydration of chlorite, thereby forming clinopyroxene in the basalt of the descending Philippine Sea Plate. Their results also indicate that the pore fluid pressure is very high at the deeper subduction interfaces where short-term SSEs occur, as assumed in the present study.

[8] *Iio et al.* [2002] reported that slip accelerated on the downward extension of a seismogenic fault leading up to large earthquakes. *Linde and Sacks* [2002] found that observations of slow deformation that occurred before several great Japanese earthquakes (the 1944 Tonankai earthquake and the 1946 Nankaido earthquake) can be explained by a model of slow preseismic slip on the downward extension of the seismic rupture zone, where the short-term SSEs occur. From the viewpoint of earthquake prediction, it is important to investigate fault behavior on deeper subduction interfaces.

[9] Many previous studies have used rate- and state-dependent friction laws to model earthquake preparation processes and cycles [e.g., *Tse and Rice*, 1986; *Rice*, 1993; *Stuart and Tullis*, 1995; *Ben-Zion and Rice*, 1997; *Kato and Hirasawa*, 1997; *Lapusta and Rice*, 2003; *Hirose and Hirahara*, 2004; *Hori et al.*, 2004]. Recently, models of SSEs have been proposed by several authors using a rate- and state-dependent friction law. SSEs can be modeled under conditions close to the stability transition. Triggered SSEs can be modeled considering a conditionally unstable cell. *Yoshida and Kato* [2003] investigated slip behavior using a 2 degrees of freedom block-slider model. Yoshida and Kato found that when one block (block 1) is unstable and the other (block 2) is conditionally unstable, SSEs can occur within block 2. *Mitsui and Hirahara* [2006] also simulated SSEs using a simplified cell model. They considered conditionally unstable cells for the transition zone and the effect of the dip angle. In these results, the amplitudes of the SSEs decrease gradually over time.

[10] Spontaneous SSEs can be reproduced in a region that is unstable but close to being stable. *Liu and Rice* [2005] performed large-scale three-dimensional (3-D) modeling of shallow subduction sequences using the Dieterich-Ruina friction law, and confirmed that SSEs occur spontaneously near the downdip end of the seismogenic zone, generated in response to the stress concentration and transient behavior. *Kuroki et al.* [2004] performed a 3-D simulation of SSEs in the Tokai region using a rate- and state-dependent friction law, considering realistic 3-D configurations of the plate interface and assigning a zone of large critical displacement within the velocity-weakening region. The ratio of the size of the generation zone to the critical size of the nucleation zone is important for the generation conditions of SSEs. *Liu and Rice* [2007] reproduced short-term SSEs using the Dieterich-Ruina friction law. They set an area of low effective normal stress and velocity weakening in the transition zone, and found that the style of slip is determined by the ratio of the width w of the generation zone to the critical cell size h^*. Furthermore, nonperiodic, short-term SSEs are generated at $w/h^* = 7$–16. Concerning an asperity model, *Kato* [2003a] clarified that SSEs can occur when the value of r/r_c, where r is radius of asperity and r_c is critical radius of asperity, is $0.25 < r/r_c < 0.5$.

[11] The other possible generation mechanism of SSEs is frictional behavior around the unstable-stable transition zone. *Shimamoto* [1986, 1989] examined steady state friction around the unstable-stable transition regime in halite by increasing the normal stress at room temperature. It was found that at very low velocity, steady state friction τ_{ss} increases with slip velocity v, whereas at low velocity τ_{ss} decreases with v, and at high slip velocity τ_{ss} increases with v. *Bréchet and Estrin* [1994] and *Estrin and Bréchet* [1996] proposed a model for the frictional sliding of ductile material with an N-shaped curve for the sliding velocity dependence of τ_{ss}. Based on 3-D modeling, *Shibazaki and Iio* [2003] simulated long-interval SSEs that occur in and below the

deeper part of the seismogenic zone for thrust earthquakes, using a rate- and state-dependent friction law with a cutoff velocity for the evolution effect that exhibits velocity weakening at low slip velocity and velocity strengthening at high slip velocity. Furthermore, by taking this frictional property into account, *Shibazaki and Shimamoto* [2007] reproduced short-term SSEs similar to those observed. Based on two-dimensional (2-D) high-resolution modeling, *Kato* [2003b] also succeeded in reproducing long-interval SSEs using a rate- and state-dependent friction law with a cutoff velocity for the evolution effect. Recently, *Beeler* [2009] proposed a more generalized frictional constitutive law for at very low velocity steady state friction τ_{ss} increases with slip velocity v; at low velocity τ_{ss} decreases with v; and at high slip velocity τ_{ss} increases with v.

[12] *Obara* [2010] investigated in detail the activity of short-term SSEs in western Japan. On the basis of tremor activity and the nature of SSEs beneath Shikoku, Obara identified three distinct segments: western, central, and eastern Shikoku. Events that occurred within longer segments were found to have longer recurrence intervals. In the above context, it is of fundamental importance to reproduce the activity of SSEs observed in southwest Japan. Therefore, in the present study we develop a model of short-term SSEs developed on the 3-D subduction interface beneath Shikoku, western Japan. We consider a rate- and state-dependent friction law with a small cutoff velocity for the evolution effect, as used previously by *Shibazaki and Iio* [2003] and *Shibazaki and Shimamoto* [2007]. It is also important to understand the mechanism of the VLF earthquakes that occur in association with SSEs. We therefore also investigate how VLF earthquakes can be reproduced numerically by considering a small patch in which friction parameters are varied.

2. Frictional Properties of the Unstable-Stable Transition Zone

[13] The three fundamental assumptions employed in the present model with regard to reproducing short-term SSEs are summarized as follows [*Shibazaki and Shimamoto*, 2007].

[14] 1. At the deeper part of the subduction interface where short-term SSEs occur, there exists an unstable-stable transition zone in which the friction law exhibits velocity weakening at low slip velocity and velocity strengthening at high slip velocity.

[15] 2. The pore fluid pressure is very high and nearly equal to lithostatic pressure at the deeper part of the subduction interface. Therefore, the stress drop is small for short-term SSEs.

[16] 3. The critical displacement is very small, as short-term SSEs yield only small amounts of fault slip and have short recurrence intervals.

[17] The amount of slip for short-term SSEs recorded in the Cascadia subduction zone is around 3 cm [*Dragert et al.*, 2001], and around 1 cm for those in the Nankai Trough [*Hirose and Obara*, 2005]. For the Cascadia and Nankai Trough SSEs, the stress drop is estimated to be 0.04–0.06 MPa [*Miyazaki et al.*, 2006] and 0.01 MPa [*Ide et al.*,

2007], respectively. A small stress drop indicates that the effective normal stress is very small because of high pore fluid pressure; otherwise, the change in the frictional coefficient $\Delta\mu$ is very small. The results of previous seismological and petrological studies suggest that pore fluid pressure is very high at the deeper subduction interfaces where short-term SSEs occur; this is also assumed in the present study. The critical displacement for the fault friction law should be very small, as short-term SSEs yield only small amounts of fault slip and have short recurrence intervals.

[18] Rate- and state-dependent friction laws have been used widely for modeling earthquake generation processes [e.g., *Dieterich*, 1981; *Ruina*, 1983]. Several types of rate- and state-dependent friction laws have been proposed [e.g., *Marone*, 1998], such as slip laws and slowness laws. The Dieterich-Ruina friction law with cutoff velocities proposed by *Okubo* [1989] is used to represent the frictional behavior that exhibits velocity weakening at low slip velocity and velocity strengthening at high slip velocity. Frictional resistance depends on both slip velocity and state:

$$\tau = \mu \sigma_n^{eff} \tag{1}$$

$$\mu = \mu_* - a \ln\left(\frac{v_1}{v} + 1\right) + b \ln\left(\frac{v_2 \Theta}{D_c} + 1\right) \tag{2}$$

where σ_n^{eff} is the effective normal stress defined as the difference between the lithostatic pressure and the pore fluid pressure P_f, v is the instantaneous sliding velocity, v_1 is the cutoff velocity for the direct effect, Θ is a state variable that characterizes the evolving state of the sliding surfaces, v_2 is the cutoff velocity for the evolution effect, and D_c is a critical displacement scaling for the evolution of the state variable. In the Dieterich-Ruina friction law, an evolution law for the state variable can be written as

$$\frac{d\Theta}{dt} = 1 - \frac{\Theta v}{D_c} \tag{3}$$

[19] The steady state friction can be written as

$$\mu_{ss}(v) = \mu_* - a \ln\left(\frac{v_1}{v} + 1\right) + b \ln\left(\frac{v_2}{v} + 1\right) \tag{4}$$

[20] The rate dependence of the steady state friction can be written as

$$\frac{d\mu_{ss}(v)}{d \ln v} = \frac{a}{1 + v/v_1} - \frac{b}{1 + v/v_2} \tag{5}$$

For the unstable-stable transition, we assume $v_2 \ll v_1$. In this case, for $v < v_2$, $\mu_{ss}(v)$ decreases with v; for $v_2 < v < v_1$, $\mu_{ss}(v)$ increases with v. In the experimental studies performed by *Shimamoto* [1986, 1989], v_2 was found to be around 10^{-5} to 10^{-7} m/s. The cutoff velocity v_2 for the evolution effect is an important parameter in determining the slip velocity of SSEs.

[21] The cutoff time Θ_* for the evolution effect can be calculated by $\Theta_* = D_c/v_2$. The cutoff time is the characteristic time of the healing process [*Bréchet and Estrin*, 1994;
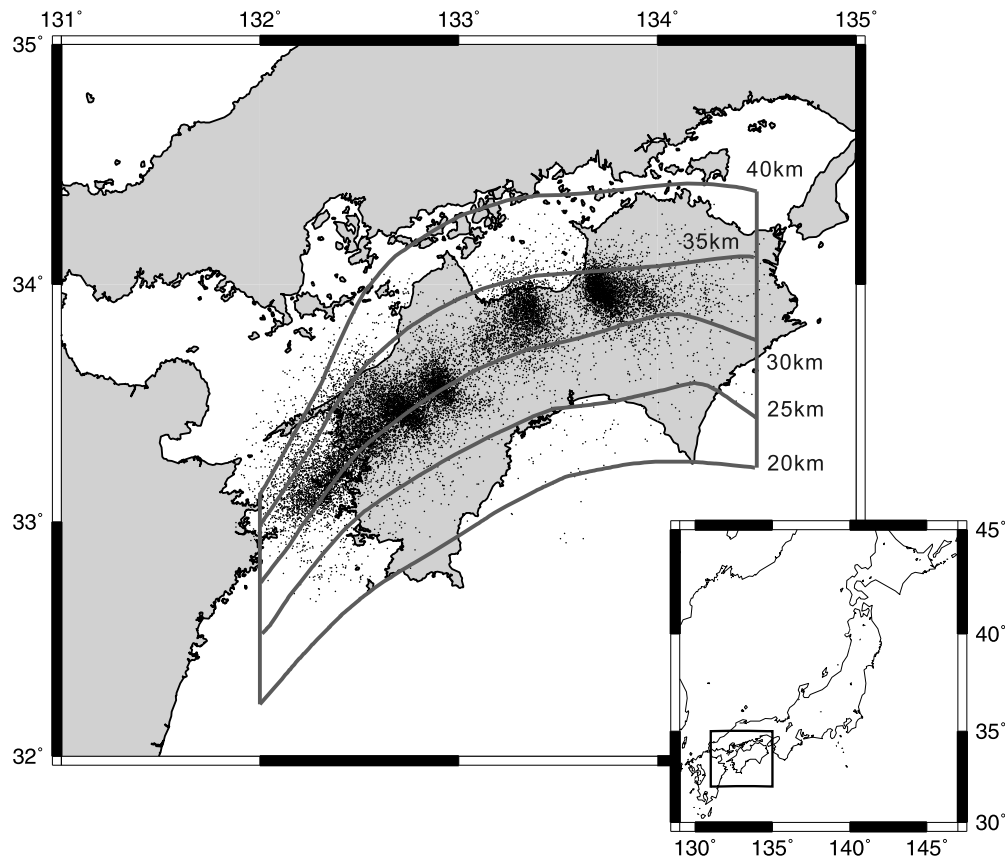
Figure 1. Configuration of the plate interface employed in modeling SSEs. Curved solid lines represent isodepth contour lines on the plate interface with the depth of 20 to 40 km. Dots indicate the epicenters of LFTs, as determined by *Obara* [2010]. The inset shows the location of the area.

Estrin and Bréchet, 1996; *Nakatani and Scholz*, 2004a, 2004b; *Beeler*, 2009]. There exist several cutoff times, depending on the mechanism of the healing process that occurs under different conditions [*Nakatani and Scholz*, 2004b]. The predominant cutoff time for healing processes in the unstable-stable transition regime where SSEs occur is possibly longer than that in the unstable seismogenic region. As discussed by *Beeler* [2009], under low effective normal stress, a long time is required for an increase in contact area between asperities. Until the required time has passed, no logarithmic change occurs. Therefore, when pore fluid pressure is high and effective normal stress is low, the cutoff time becomes long and cutoff velocity becomes low.

3. Slow Slip Events on a 3-D Subduction Plate Boundary

3.1. Activity of SSEs and Low-Frequency Tremors Beneath Shikoku

[22] The activity of short-term SSEs in western Japan has been investigated in detail by *Obara* [2010]. Here, we briefly summarize the results of this study in terms of the activity of short-term SSEs beneath Shikoku. Three distinct segments along the deep subduction zone are recognized based on tremor activity: western, central, and eastern Shikoku. The activity beneath western Shikoku is the highest in all of southwestern Japan. The length of this

segment is around 100 km, the recurrence interval of events is around 3–6 months, the propagation velocity of SSEs is around 10 km/d, and the moment magnitudes and fault slips of SSEs are around 6.0 and 1–2 cm, respectively. Beneath eastern and central Shikoku, the length of the segment is around 50 km and the recurrence interval of events is around 2–3 months. An observed characteristic of low-frequency tremors is that their area (length and width) in the segment beneath western Shikoku is greater than that beneath central and eastern Shikoku. This difference may affect the occurrence of SSEs at each segment.

3.2. Loading Processes and Elastic Interactions

[23] To investigate the activity of SSEs observed beneath Shikoku, we develop a model of short-term SSEs on the 3-D subduction interface. The assumed configuration of the plate interface is shown in Figure 1. In developing this configuration, we referred to depth contours of the distribution of intraplate earthquakes in the Philippine Sea Plate, as provided by *Nakamura et al.* [1997]. For depths of 25–35 km, we use the contour lines provided in this earlier study, in which a discontinuity is reported in the depth contour of intraplate earthquakes at a depth of 40 km beneath Shikoku. Therefore, we modified the contour line at a depth of 40 km to be smooth near the site of the discontinuity. Because *Nakamura et al.* [1997] did not construct contour lines at depths greater than 40 km in the model region, we added a
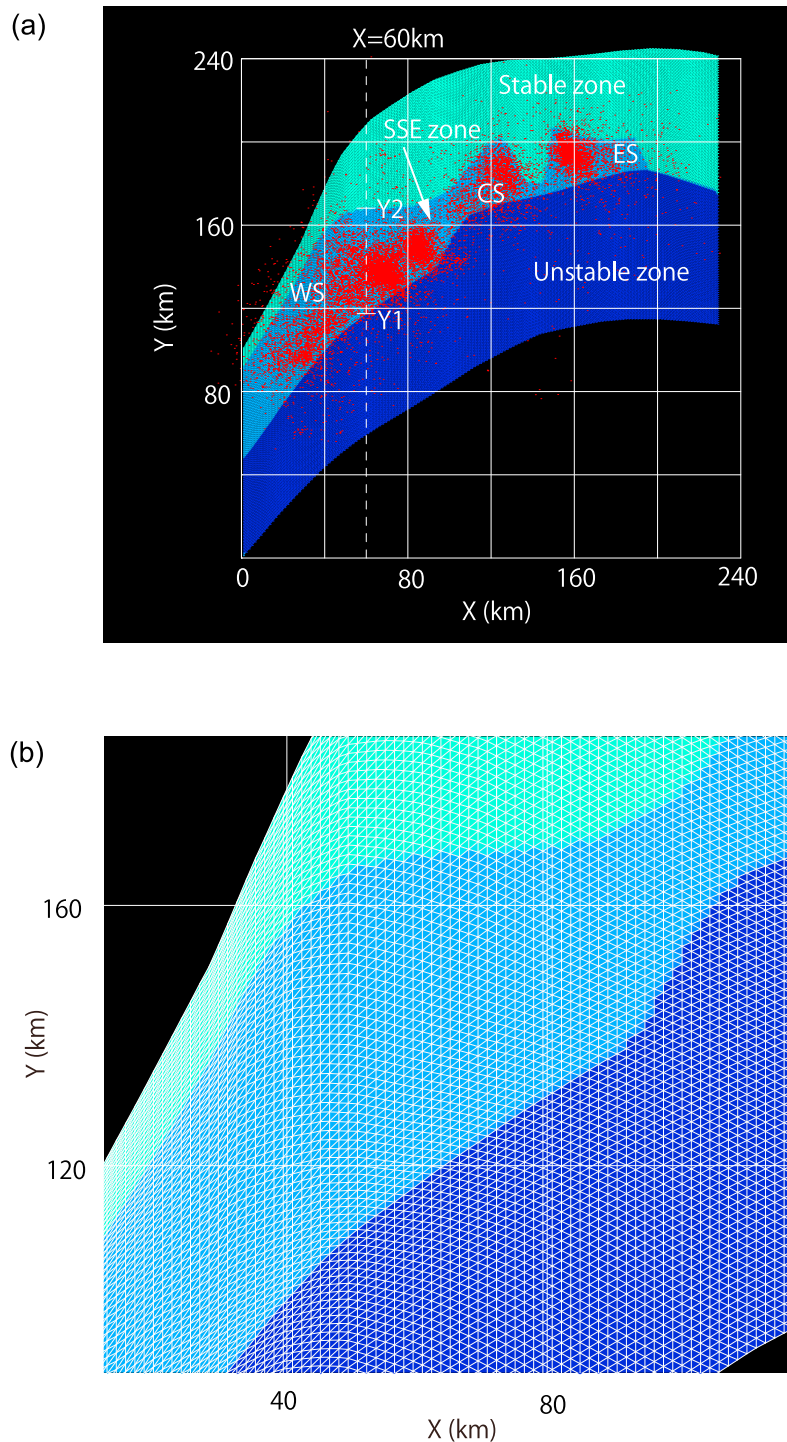
Figure 2. Map views of 3-D plate interface for modeling SSEs. *X* and *Y* axes indicate distances along the W-E and S-N directions. (a) SSE zone, stable zone, and unstable zone. Red dots indicate the epicenters of LFTs, as determined by *Obara* [2010]. SSE zone includes the high-activity region of LFTs and is divided into three segments: western (WS), central (CS), and eastern (ES). (b) Triangular meshes for the western segment.

contour line at a depth of 45 km by smoothly extrapolating the plate interface (25–40 km) downward to this depth. We then subtracted 5 km from each depth, as the contour lines proposed by *Nakamura et al.* [1997] represent the depth of intraplate earthquakes, whereas the actual depth of the plate interface is shallower. The dip angle of the plate interface increases from central to western Shikoku. In the present study, we model SSEs but do not consider interactions between SSEs and large megathrust earthquakes. Therefore, we do not take into account the entire seismogenic region:
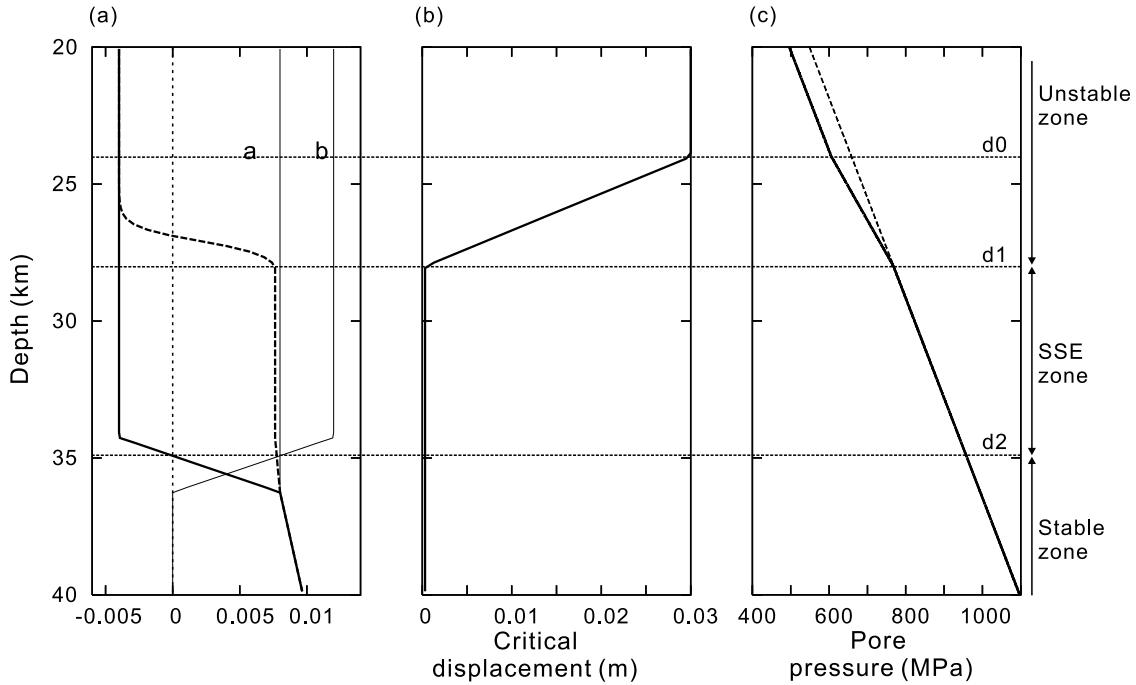
Figure 3. Depth distributions of (a) the constitutive law parameters a, b, (b) critical displacement D_c, and (c) the pore fluid pressure P_f at $X = 60$ km in Figure 2a. The thick solid line and dashed line in Figure 3a show the depth distributions of $d\mu_{ss}(v)/d \ln v$ at $v = 10^{-10}$ m/s and 10^{-5} m/s, respectively. The thick solid line and dashed line in Figure 3c shows the pore fluid pressure and the lithostatic pressure. The SSE zone is defined as the depth range from $d1$ and $d2$, which corresponds to the range between $Y1$ and $Y2$ in Figure 2a.

the depth range of the model space is limited to between 20 and 40 km.

[24] At the Nankai subduction zone, the Philippine Sea Plate is subducting beneath the Amurian Plate toward from N55W to N60W at a relative velocity of around 6 cm/yr [*Heki and Miyazaki*, 2001; *Miyazaki and Heki*, 2001]. A curved plate interface as shown in Figure 1 is divided into triangular elements. Now we consider a long-term average relative slip velocity at each element. We take the x axis to be the W-E direction and the y axis to be the S-N direction as shown in Figure 2a. Z axis is taken to be an upward direction. The long-term average relative slip velocity of the ith element has three components: $\mathbf{v}_{pl,i} = (v_{pl1,i}, v_{pl2,i}, v_{pl3,i})$. The term $|\mathbf{v}_{pl,i}|$ is fixed at $v_{pl} = 6$ cm/yr for all elements. Based on the direction of plate convergence, $v_{pl1,i}/v_{pl2,i} = -\tan 55°$ is assumed. Furthermore, $\mathbf{v}_{pl,i}$ must be parallel to the surface of a triangular element. Given the three conditions outline above, $\mathbf{v}_{pl,i}$ can be determined.

[25] We fix the direction of fault slip to be $\mathbf{v}_{pl,i}/v_{pl}$. Therefore, we only consider the shear stress τ_i on the i element along the direction of $\mathbf{v}_{pl,i}/v_{pl}$ on the fault. The shear stress τ_i on the i element is accumulated by the delay of the fault slip u_{i_s} from the motion $v_{pl}t$:

$$\tau_i = \sum_{i_s} k_{i-i_s}\left(v_{pl}t - u_{i_s}\right) - \frac{G}{2\beta}\frac{du_i}{dt} \qquad (6)$$

where k_{i-i_s} is the elastostatic kernel that is the stress at the center of gravity of the i triangular element caused by uniform slip along the direction $\mathbf{v}_{pl,i}/v_{pl}$ over the i_s triangular

element. The centers of gravity of the triangular elements are taken to be the nodes (collocation points). We use the program for calculating the kernel for triangular elements used by *Stuart et al.* [1997]. The first term in the equation represents the tectonic loading due to relative plate motion; the second term is the seismic radiation damping introduced by *Rice* [1993]. For a slip velocity of 10^{-6} m/s, the value of the second term is around 4 Pa; therefore, in the present case this term is negligible. For simplicity, we do not consider the effect of normal stress changes. By solving the coupled constitutive equations (1)–(3) and the equation of tectonic loading (6) using the Runge-Kutta method [*Press et al.*, 1992], the slip velocity and shear stress histories can be obtained. We assume that no slip occurs outside the model fault area shown in Figure 2a.

3.3. Parameter Setting

[26] Figure 2a shows the distribution of LFTs obtained by *Obara* [2010], along with the generation zone of SSEs, unstable zone, and stable zone. Figure 2b shows the triangular mesh for the western segment. The number of mesh points in the entire region in Figure 2a is 100 (dip direction) × 160 (horizontal direction) = 16,000. Therefore, the region contains 32,000 triangular elements. The distances between nodes in adjoining triangular elements change with position, but are less than around 1.2 km for most elements, although larger distances are found in the deeper part beneath western Shikoku (maximum, 1.49 km).

[27] Figure 3 shows the depth distribution of the constitutive law parameters a, b, D_c, and pore fluid pressure P_f at

Table 1. Model Parameters at the Generation Zone of SSEs in the 3-D Simulation

Symbol	Parameter	Value
v_1	Cutoff velocity for the direct effect	1.0 m/s
v_2	Cutoff velocity for the evolution effect	$1.0^{-6.5}$ m/s
D_c	Critical displacement	0.3 mm
σ_n^{eff}	Effective normal stress	0.42 MPa
a	Parameters for rate- and state-dependent friction law	0.008
b		0.012
G	Rigidity	30 GPa
v_{pl}	Relative velocity of plate motion	6 cm/yr

$X = 60$ km in Figure 2a. The effective normal stress σ_n^{eff} is defined as the difference between lithostatic pressure and pore fluid pressure P_f, as shown in Figure 3c. The depth range is taken to be 20–40 km. In the present case, the zone of main slips of SSEs lies in the depth range of d1 to d2, where $d\mu_{ss}(v)/d \ln v \approx a - b < 0$ for a low slip velocity, but $d\mu_{ss}(v)/d \ln v \approx a > 0$ for a high slip velocity. A frictional stable zone exists below the SSE zone. For simplicity, we use the same values of D_c and σ_n^{eff} for the stable zone as used for the SSE zone. Y1 and Y2 in Figure 2a correspond to d1 and d2 in Figure 3. Figure 2a was created by mapping SSE zone (defined by the depth range from d1 to d2) on the XY plane.

[28] We set the three generation segments of SSEs based on the LFT distribution such that the segments contain many LFT epicenters by changing d1 and d2 with horizontal distance X. The western segment is the largest in terms of length and width, and appears to contain patches with very high tremor activity; however, these patches are not isolated. Therefore, we take the western segment to be a single large segment. The central and eastern segments appear to be isolated; consequently, we set narrow widths for the connecting zones between the western, central, and eastern segments.

[29] Table 1 lists the parameters employed for the generation zone of SSEs. The effective normal stress σ_n^{eff}, the cutoff velocity v_2 for the evolution effect, and the critical displacement D_c are the important parameters characterizing the occurrence of SSEs. We set the value of the cutoff velocity v_2 to $10^{-6.5}$ m/s, higher than the average slip velocity of SSEs (around 10^{-7} m/s) [*Hirose and Obara*, 2005].

[30] When considering a rate- and state-dependent friction law, the stress drop defined as the difference between the initial and final stresses can be approximated by $\Delta\tau \approx -(a - b)\sigma_n^{eff} \ln(v_{max}/v_{ini})$, where v_{max} and v_{ini} are the maximum slip velocity and initial slip velocity, respectively. We assume that $v_{max} = 10^{-7}$ m/s and $v_{ini} = 10^{-10}$ m/s. When $\Delta\tau = 0.01$ MPa [e.g., *Ide et al.*, 2007], $(b - a)\sigma_n^{eff}$ is estimated to be 0.0014 MPa. Assuming that $b - a = 0.004$, σ_n^{eff} is estimated to be around 0.35 MPa. In the present study, we set

σ_n^{eff} to 0.42 MPa. *Nakata et al.* [2008] estimated the value of $a\sigma_n^{eff}$ to be 0.0013 MPa for the SSE zone in eastern Shikoku. Assuming a value for a of 0.008, σ_n^{eff} is calculated to be 0.16 MPa. Therefore, the assumed value of σ_n^{eff} is largely consistent with the results of *Nakata et al.* [2008]. The value of the critical displacement is set to be sufficiently small for the reproduction of the SSEs. At larger values of critical displacement, the SSEs become very slow or stable slidings occur.

[31] The critical nucleation size is calculated using the equation $h_* = 2GD_c/[\pi(b - a)\sigma_n^{eff}]$ [*Rice*, 1993], and the nucleation length scale is calculated by $L_b \approx GD_c/b\sigma_n^{eff}$ [*Dieterich*, 1992; *Rubin and Ampuero*, 2005]. Node intervals must be less than these values. In the present case, $h_* = 3.4$ km and $L_b = 1.79$ km. The largest node interval in the present study is 1.49 km; all intervals are less than $L_b = 1.79$ km.

3.4. Numerical Results

[32] Figure 4 shows the results of a numerical simulation of the slip velocity distribution on the curved plate interface over time from $t = 2.99108$ to 3.67773 years. During this period, two large SSEs occur within the western segment. A very slow slip region (dark blue region in Figure 4) represents the locked seismogenic region. Around $t = 3.04764$ year, a larger slow slip event nucleates at the western segment and propagates bilaterally. The maximum slip velocity reaches 10^{-6} m/s. This event also propagates to the east and slow slips occur at the central and eastern segments ($t = 3.05734$, and 3.08938 years). The slip velocity then becomes very low in the region where the SSE occurs. At $t = 3.33277$ years, a small event occurs at the left-hand edge of the western segment, and then, at $t = 3.36981$ and 3.41019 years, small events occur in the central and eastern segments. The slip velocity for these smaller events is low compared with that for the larger events within the western segment. It should be noted that the eastern part of the western segment remains unruptured although small SSEs occurred in the surrounding region. At $t = 3.49420$ years, another large SSE nucleates at the western segment and propagates bilaterally. The recurrence interval of larger events at the western segment is around 6 months. The recurrence interval for smaller events at the central and eastern segments is around 3 months, shorter than that for larger events.

[33] Figures 5a and 5b shows the changes in slip velocity over time (from $t = 1$ to 6.5 years) along the lines of depths of 31.5 and 33 km. The very narrow straight zones with white to red colors indicate SSEs. Dark blue zones indicate low-slip-velocity zones during inter-SSE periods. From Figure 5b, we can confirm the stable slips between the western and central segments and the central and eastern segments. SSEs have different characteristics in the three segments. In the eastern and central segments, events with a relatively small length (around 50 km) occur at intervals of 2–3 months. The larger SSEs in the western segment are

Figure 4. Snapshots of slip velocity distribution from $t = 2.99108$ to 3.67773 years on the curved plate interface at each time step (year) for several SSEs. (top) The slip velocity distribution at $t = 3.04977$ years is shown with the spatial scale and the scale of slip velocity. The X and Y axes indicate the distances in the W-E and S-N directions, respectively. (bottom) The numbers represent the time in years. Dark blue color indicates the locked region with low slip velocity. In the shallower part (i.e., seismogenic region), the slip velocity is constantly very low. In the deeper part, the slip velocity is close to the velocity of relative plate motion. Yellow and red colors indicate high-slip-velocity regions within which SSEs are generated.
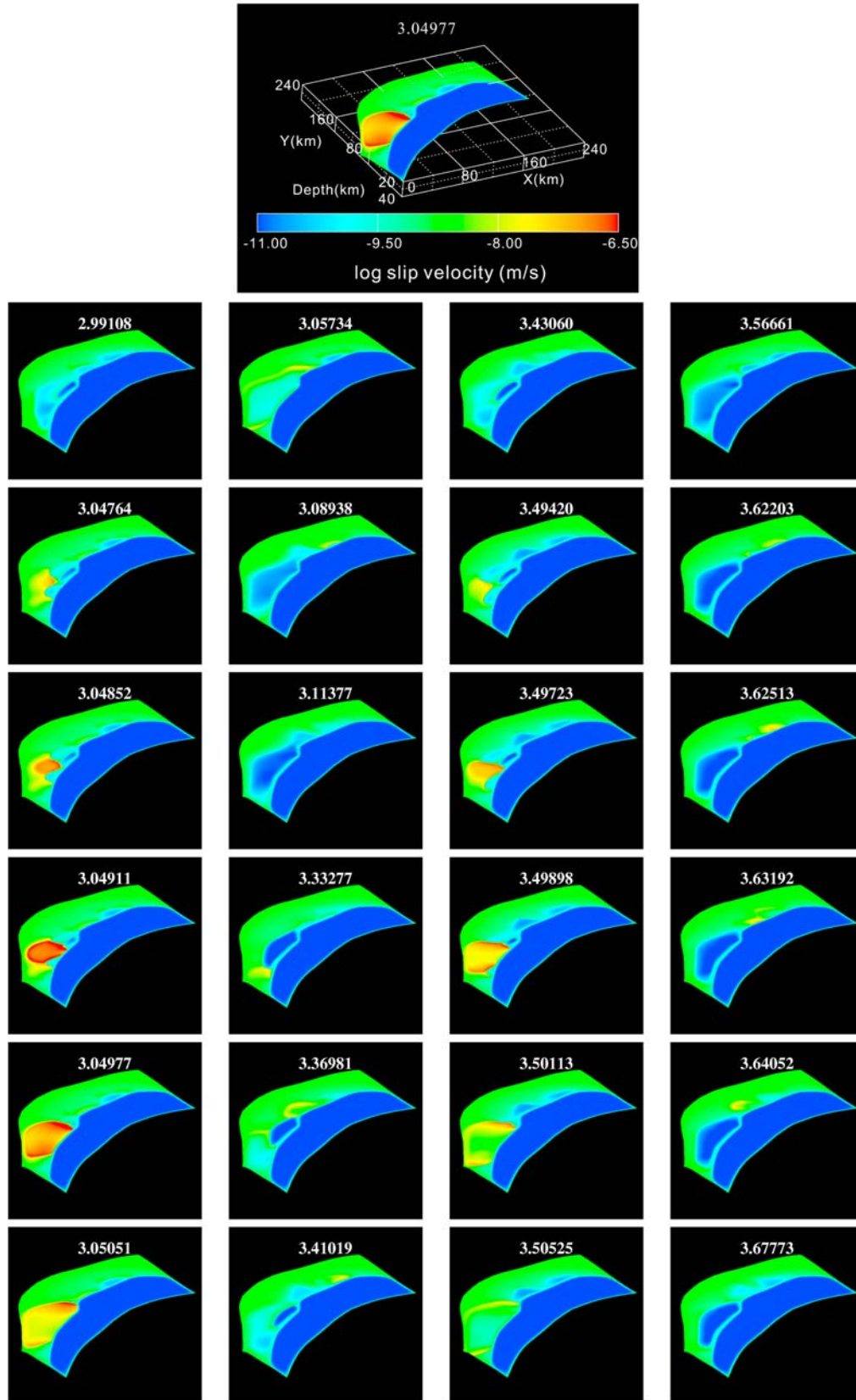
Figure 4
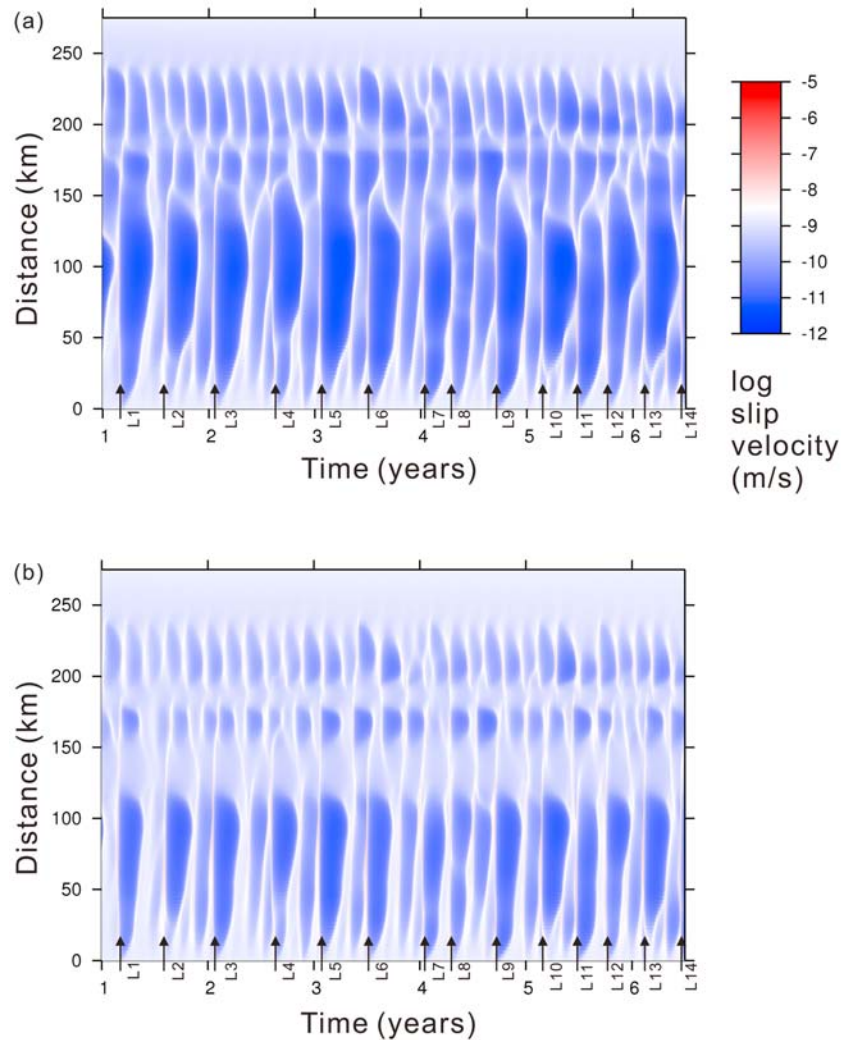
Figure 5. Slip velocity distribution along the horizontal curved line from $t = 1$ to 6.5 years at depths of (a) 31.5 km and (b) 33 km. The very narrow straight zones with white to red colors indicate SSEs. Blue regions represent low-slip-velocity zones. L1–14 are large events that correspond to the moment rate functions shown in Figure 6a.

indicated by L1–14. Slow slip events in the western segment have longer recurrence intervals (3–8 months) than those in the central and eastern segments. The length of the SSE reaches 100 km in the western segment. Some SSEs rupture both the western and central segments or the central and western segments. Rare SSEs (L1 and L5) rupture all three segments.

[34] Figure 6a shows temporal changes in the moment rate, defined as $G\sum_i v_i \Delta S_i$, where v_i and ΔS_i are the slip velocity and the area of the ith triangular element, respectively, as located in the SSE zone. The L1–14 SSEs, which have a maximum moment rate greater than 2.0×10^{12} Nm/s, occur with a recurrence interval of 3–8 months. L1–14 correspond to those shown in Figure 5. Figure 6b shows the cumulative moment obtained by integrating the moment rate. We can confirm that small steps in the cumulative moment correspond to the occurrences of the L1–14 SSEs. The amount of moment release for the L1–14 SSEs is around 1.0×10^{18} Nm, for which the moment magnitudes

are M_w 5.9, consistent with observed values. During the intervals between larger events, we can confirm some small-amplitude events that correspond to the small events in the western, central, and eastern segments.

[35] Figure 7 shows the depth distribution of slip with time at $x = 60$ km. Slips at $t = 3$ years were set to zero. The amount of fault slip for larger events is around 1 cm. In deeper regions, slip increases steadily with time, the amount of which is nearly equal to $v_{pl}t$. The fault is locked in the upper seismogenic zone; therefore, the total amount of fault slip within the SSE zone is much less than the relative plate motion $v_{pl}t$. We observe that at $t = 3.05$, 3.50, and 4.05 years, larger events (L5–7) that rupture the entire zone of SSEs occur. From 6a, the maximum moment rates of these events exceeds 2.0×10^{12} Nm/s. During the intervals between these events, very small SSEs occur at $t = 3.34$ and 3.8 years. The maximum moment rates of these events are very small compared with those of L1–14. For observed SSEs in the western segment, tremor activity for which SSEs are not
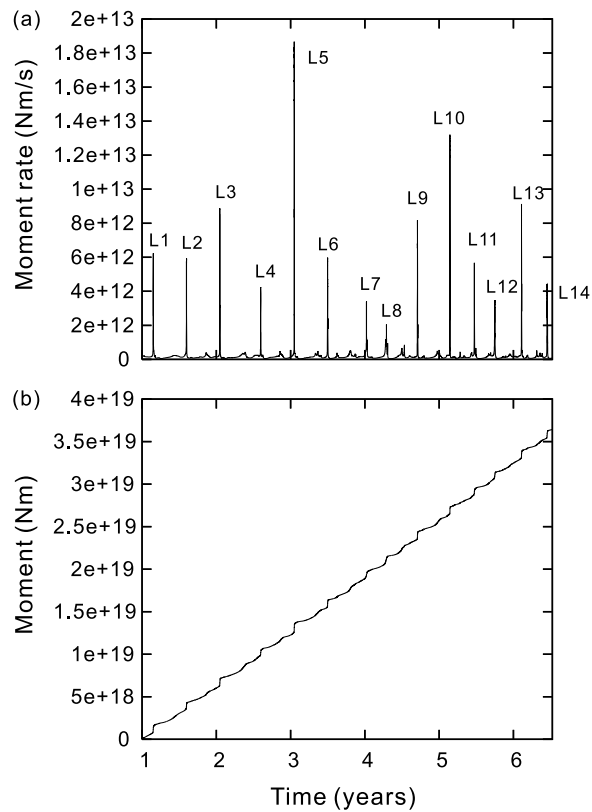
Figure 6. (a) Temporal changes in moment rate, as calculated by summing the moment rate at the elements in the entire SSE zone. (b) Cumulative moment obtained by integration of the moment rate. L1–14 indicate large events that correspond to those in Figure 5.

observed by tiltmeters occurs during the periods between large SSEs that are observed by tiltmeters. Our model can reproduce the modes of the SSEs similar to those observed beneath Shikoku.

[36] Figure 8 shows the changes in slip velocity for the four SSEs (L2, 5, 7, and 13). The L2 event nucleates slowly in the western part of the western segment, and propagates unilaterally to the east at a speed of 10–20 km/d. It takes around 6 days for this event to reach completion. In actual SSEs, a nucleation phase appears to occur when tremor activity is high within a certain limited area over a period of several days [*Obara*, 2010]. The L5 event starts in the center of the western segment and propagates bilaterally with a speed of 50 km/d, and it propagates to the central segment at a speed of 10 km/d. Subsequently, a small SSE occurs within the eastern segment. The L7 event starts in the eastern part of the western segment and propagates slowly and bilaterally at a speed of 5 km/d. This SSE is complex: two subevents occur during its propagation to the west. The L13 event starts in the western segment and propagates to the central segment at a speed of 25 km/d. In actual observations, SSEs sometimes extend over two or three segments. For example, *Obara* [2010] reported that some actual SSEs rupture both the western and central segments or the central and western segments. Rare SSEs rupture all three segments.

[37] We also consider a relatively simple case in which the width of the generation zone of SSEs is set such that it is wider beneath the western part of Shikoku than beneath the central and eastern parts. This configuration is able to reproduce events beneath western Shikoku with longer lengths in the along-strike direction and longer recurrence times, as well as events beneath eastern and central Shikoku with smaller lengths in the along-strike direction and smaller recurrence times. The simulated activity is similar to that
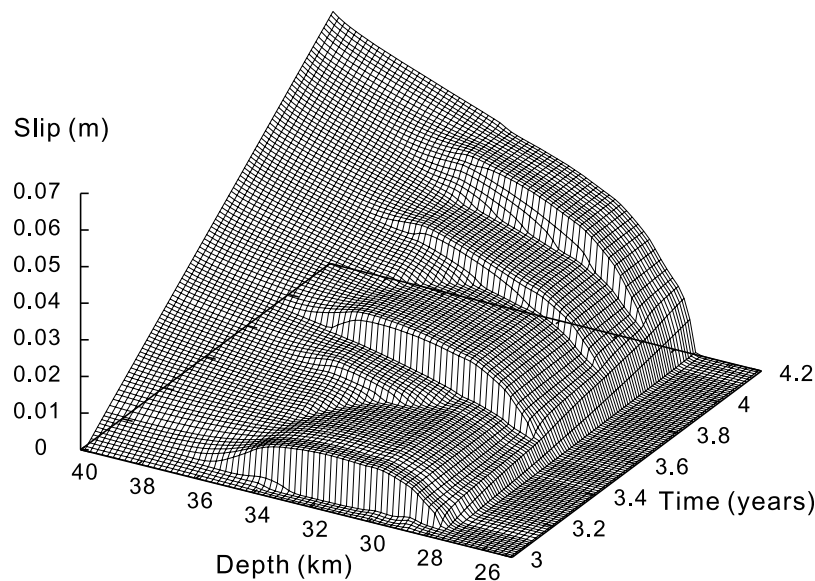
Figure 7. Temporal changes in the fault slip distribution with depth at $X = 60$ km in Figure 2a. In the deepest portion, fault slip shows a near-constant increase. In the shallower part, slip is close to zero. Between these two regions, SSEs occur repeatedly. SSEs at $t = 3.05$, 3.50, and 4.05 years correspond to L5–7 in Figure 5. Between theses events small very slow events are observed at $t = 3.34$ and 3.8 years. The amount of fault slip for large SSEs is around 1 cm.
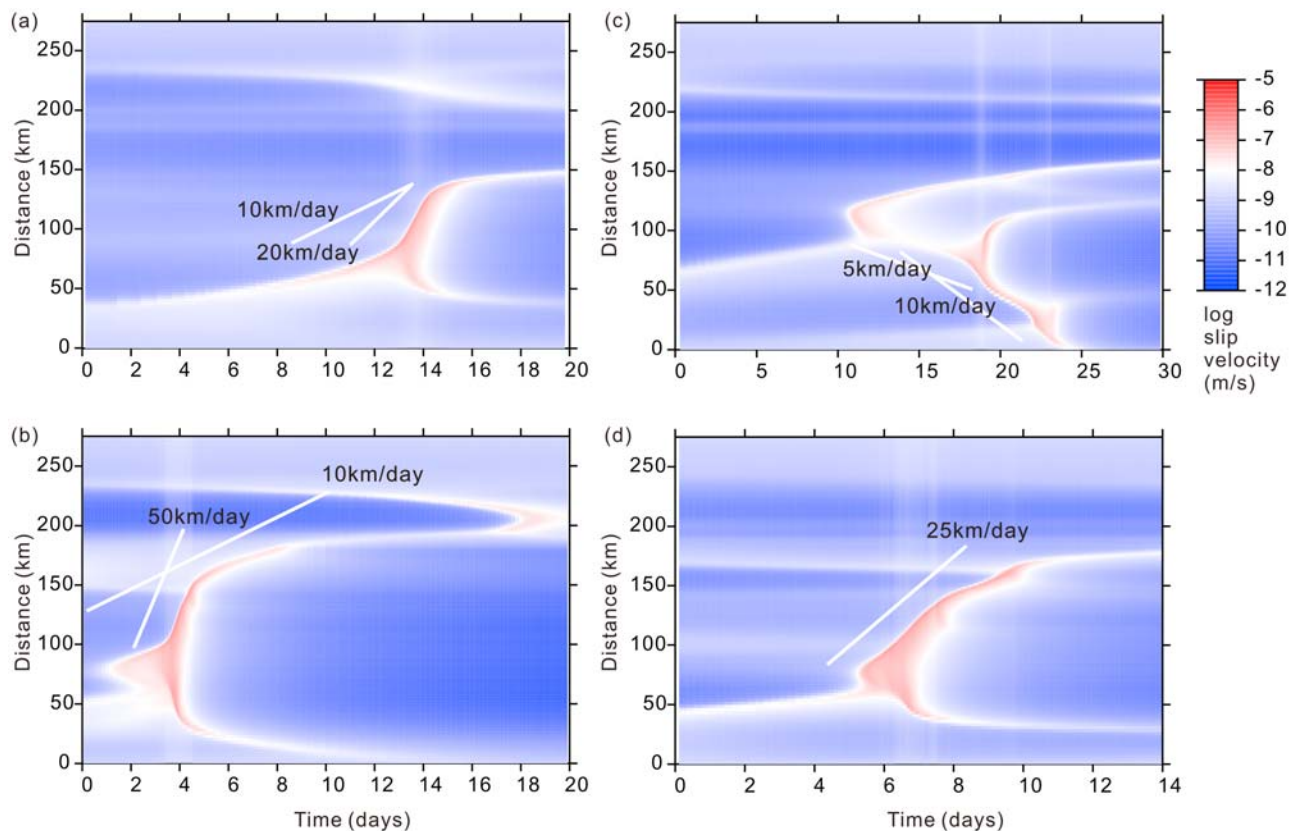
Figure 8. Slip velocity distribution over time at a depth of 31.5 km for events (a) L2, (b) L5, (c) L7, and (d) L13.

observed; however, in the model results there is no clear segmentation beneath central and eastern Shikoku. Multi-segment events occur frequently in the case where we increased the widths of connecting zones between the western, central, and eastern segments. Therefore, in modeling the realistic activity of SSEs, it is necessary to consider nonuniform frictional properties inferred from the distributions of LFTs.

[38] We examined how the solutions varied in response to slight changes in the node intervals, and found that the solutions arrived at after several years of the simulation are different from those shown in Figure 5. However, even with changes in the node intervals, we reproduced SSEs with the same characteristics in terms of recurrence interval, velocity, slip velocity, etc. The differences observed in the solutions may reflect the fact that the node intervals were not enough small. In the case of a triangular mesh, changes in node intervals result in slight changes in the form of the plate interface. This may be another possible cause of the differences among the solutions obtained with different node intervals.

4. Two-Dimensional Modeling of Low-Frequency Earthquakes

[39] We also attempt to model the VLF earthquakes observed by *Ito et al.* [2007], which were accompanied by short-term SSEs. They proposed a possible scenario for the occurrence of these VLF earthquakes, in which relatively

strongly coupled patches of VLF earthquakes are surrounded by a region of short-term SSEs. *Ide et al.* [2007] proposed the scaling law in which the moment M_0 of slow earthquakes is proportional to duration T. They discussed scaling laws between the characteristic propagation velocity and event size. In the case where the stress drop is constant, fault slip Δu increases with event size L. In this case, $M_0 \propto L^3 \propto T$; therefore, $L/T \propto 1/L^2$. In the case where fault slip Δu is constant, $M_0 \propto L^2 \propto T$; therefore, $L/T \propto 1/L$. These results suggest that the characteristic propagation velocity L/T increases with decreasing event size. Although this relationship has not been confirmed from observations, VLF earthquakes are assumed to be a local high-speed rupture, and are expected to represent events with much higher slip velocity than that for SSEs, as these events radiate seismic energy. To model a local high-speed rupture with high slip velocity, it is necessary to vary the constitutive law parameters at the patch of VLF earthquakes. Because we require a small grid size, we consider a 2-D model and set a local patch in which the constitutive law parameters are varied.

4.1. Loading Processes and Elastic Interactions

[40] We now consider a quasi-dynamic analysis that assumes a thrust fault in a 2-D elastic half-space, as illustrated in Figure 9. The fault plane is located along the ξ axis, and the direction of slip is along the ξ direction. The free surface is located on the $z = 0$ plane. A fault plane is divided into cells of length $\Delta\xi$. The i cell occupies the region $(i-1)\Delta\xi \leq \xi \leq i\Delta\xi$ ($i = 1, \cdots M$). The slip is assumed to be constant within
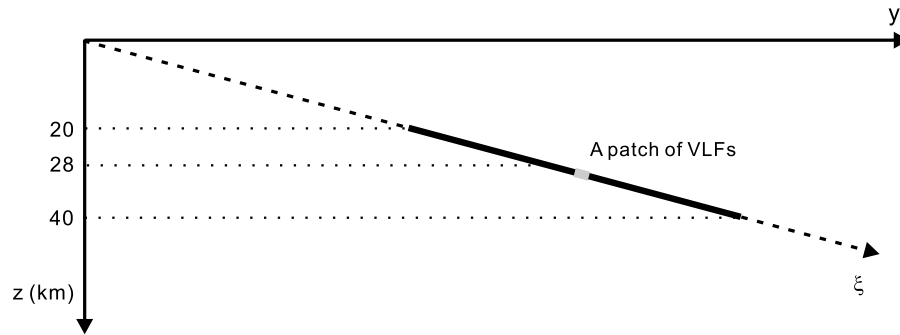
Figure 9. Model space of a thrust fault in a 2-D elastic half-space. The ξ axis is taken to be the downdip direction of the fault. The fault plane is divided into equal segments of $\Delta\xi = 0.018$ km. The depth range of the fault zone is taken to be 20–40 km. The generation zone of SSEs is taken to be 28 to 38 km. There exists a small patch in the zone of SSEs for VLF earthquakes.

each cell. The shear stress τ_i on the i cell on the fault is accumulated by delay of the fault slip $u_{(i_s)}$ from the relative plate motion, following equation (6). In this case, k_{i-i_s} in equation (6) is the elastostatic kernel, which is the stress at the center of the i cell caused by the uniform slip over the i_s cell. Because VLF earthquakes are seismic events, the term that represents radiation damping is important in considering the approximate effect of inertia.

4.2. Parameter Setting and Numerical Results

[41] As an example, we consider an M_w 3.5 VLF earthquake with a seismic moment of 2.24×10^{14} Nm. When assuming a circular crack model and $\Delta\sigma = 0.01$ MPa, the crack radius a is calculated to be 2140 m using a formula of

$M_0 = (16/7)\Delta\sigma a^3$. Assuming the duration to be 20 s, rupture velocity is calculated to be around 100 m/s. The following relationship between maximum slip velocity and rupture velocity was obtained theoretically by *Ida* [1973] under the condition that a mode 2 shear rupture propagates at a constant velocity v_r: $\dot{u}_{max} = (\gamma\Delta\sigma_b/G)v_r$, where γ is an order of unity and $\Delta\sigma_b$ is the breakdown strength drop, defined as the difference between the peak stress and frictional stress. Assuming $\Delta\sigma_b = 2\Delta\sigma$, $\dot{u}_{max} = 3 \times 10^{-5}$ m/s. In this case, $\dot{u}_{max}$ is 100 times faster than the cutoff velocity used in the SSE modeling.

[42] When $\Delta\sigma = 0.1$ MPa, crack radius a is calculated to be 993 m. In this case, rupture velocity is calculated to be around 50 m/s. Assuming $\Delta\sigma_b = 2\Delta\sigma$, $\dot{u}_{max} = 1.5 \times 10^{-4}$ m/s. In this
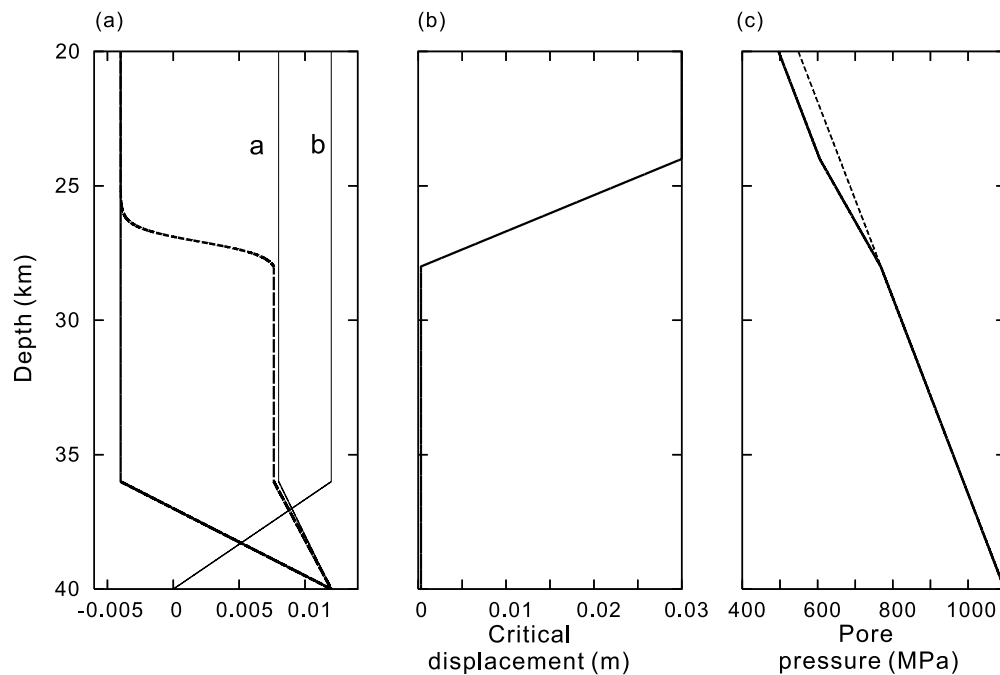
Figure 10. Depth distributions of (a) the constitutive law parameters a, b, (b) critical displacement D_c, and (c) the pore fluid pressure P_f. The thick solid line and dashed line in Figure 10a show the depth distributions of $d\mu_{ss}(v)/d\ln v$ at $v = 10^{-10}$ m/s and 10^{-5} m/s, respectively. The generation zone of SSEs is taken to be 28 to 38 km. The thick solid line and dashed line in Figure 10c show the pore fluid pressure and the lithostatic pressure.

Table 2. Model Parameters in the Fault Patch of VLF Earthquakes in 2-D Simulations[a]

Case	w (km)	v_2 (m/s)	D_c (mm)	σ_n^{eff} (MPa)
1	3.86	$1.0 \times 10^{-6.5}$	0.015	0.42
2	3.86	1.0	0.03	0.42
3	1.55	$1.0 \times 10^{-6.5}$	0.30	4.2

[a]Parameters are w, fault patch length of VLF earthquakes; v_2, cutoff velocity for the evolution effect; D_c, critical displacement; σ_n^{eff}, effective normal stress.

case, $\dot{u}_{max}$ is 500 times faster than the cutoff velocity used in the SSE modeling. In the present study, we consider a 2-D fault, and the fault patch length of VLF earthquakes is set to 3.86 and 1.55 km.

[43] The depth range of the fault zone for the simulation is taken to be 20–40 km (Figure 9). The depth range of SSEs is approximately 28–38 km. We take the grid size and grid number to be 18 m and 4000, respectively; dip angle is 15°. Figure 10 shows the depth distributions of the constitutive law parameters a, b, critical displacement D_c, and pore fluid pressure P_f. In these distributions, the patch of VLF earthquakes is not considered. The values of the constitutive law parameters for the generation zone of SSEs are the same as those listed in Table 1.

[44] There are several ways to reproduce locally high-speed rupture. Table 2 lists the investigated cases, in which the size and constitutive law parameters of the patch are varied. First, we take a smaller critical displacement for the patch. Second, we take a larger cutoff velocity for the patch; however, in this case, if we do not take a smaller critical displacement for the patch the rupture velocity shows no significant increase. Therefore, we take a smaller critical displacement. Third, we take a larger effective normal stress for the patch, maintaining the same value of critical displacement. In addition, we take a smaller patch size. In this case, the fracture energy of the fault becomes highest at the patch.

[45] For these three approaches to produce local high-speed rupture, the values for the ratio of w/h^* (ratio of the length of the patch of the VLF earthquake to the critical size) need to be relatively high: 22.7 (case 1); 11.4 (case 2); and 4.6 (case 3). *Liu and Rice* [2007] confirmed that seismic events occur at higher values of w/h^*. In the present model, we reproduce VLF earthquakes considering a local patch with high values of w/h^*, that is located between SSE zones.

[46] Figure 11 shows the spatiotemporal development of the SSE in case 1, including VLF earthquakes. First, a fast, local event occurs at the local patch with a propagation velocity of around 10 m/s. Then, with gradual extension of slip in the region, several fast events occur repeatedly at the local patch. Figure 12a shows the moment rate function for the SSE, as also shown in Figure 11. The moment rate is calculated as $G\sum_i v_i \Delta\xi$, where v_i and $\Delta\xi$ are the slip velocity of the ith element and element length, respectively. Therefore, the unit of moment is N/s. To obtain the moment rate on a 2-D fault, we need to multiply the calculated moment rate by the horizontal length of the fault. Several fast events (VLF earthquakes) occur repeatedly during a single SSE. Figure 12b shows an expanded time scale for the single event indicated by the arrow in Figure 12a. The moment rate of this VLF earthquake shows a gradual change over time.

[47] Figure 13a shows the moment rate function for one typical SSE in case 2, where the cutoff velocity for the evolution effect for the patch is set to 1.0 m/s. A very fast VLF earthquake occurs, followed by repeated events during one event. Figure 13b shows an expanded time scale for a single event indicated by arrow in Figure 13a. The moment rate function for a single event shown is very simple: it increases and decreases rapidly. The shape of the moment rate function is somewhat different from that for the lower cutoff velocity. The fast slip events reproduced in this case can be regarded as usual fast rupture propagation, although the stress drop is small. In cases 1 and 2, an SSE generally starts with a VLF earthquake, and repeated VLF earthquakes
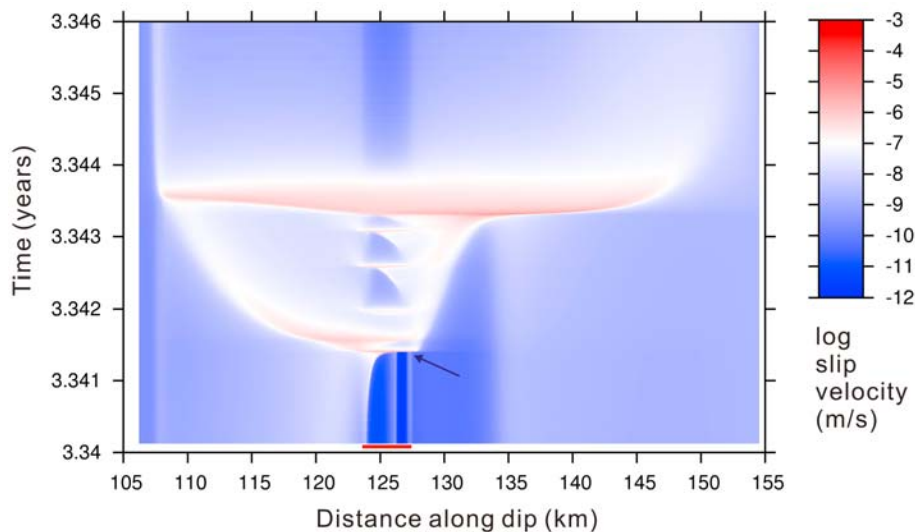
Figure 11. Spatial distribution of slip velocity over time for an SSE in case 1. The red bar indicates the location of the patch of VLF earthquakes.
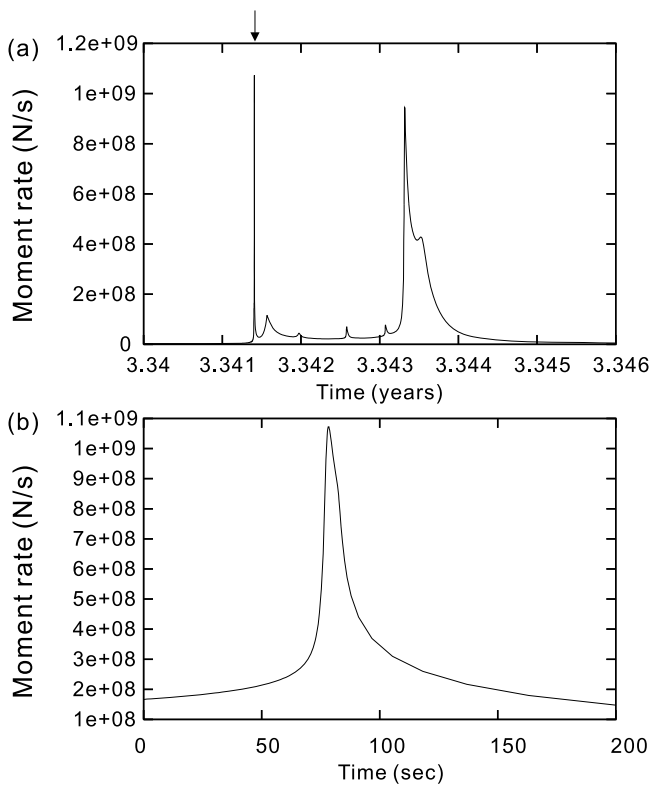
Figure 12. (a) Moment rate for the SSE on a 1-D fault in case 1, as shown in Figure 11. The unit of moment rate is N/s, as we consider 1-D fault slip. (b) Moment rate with an extended time scale for the VLF event indicated by the arrow in Figure 12a and in Figure 11.

occur as part of the SSE; very few VLF earthquakes occur as events that are independent of the SSE.

[48] Figure 14a shows the spatiotemporal development of SSEs over 0.3 year in case 3, where the effective normal stress for the patch is 10 times that of the surrounding region. Figure 14b shows the large SSE at $t = 12.569$ years with an expanded time scale. In this case, SSEs occur in the deeper and upper parts of the patch, but the patch remains unruptured and serves as a barrier for the SSE. Finally, a fast slip event occurs at the patch; slip then propagates into the entire zone of SSEs. Figure 15a shows the moment rate function for the SSE, as also shown in Figure 14b. Figure 15b shows an expanded time scale for the single event indicated by the arrow in Figures 15a and 14b. As shown in Figure 15b, the source time function of the event increases rapidly, corresponding to rupture at the patch; however, the moment is subsequently slowly released. Although this model also can produce VLF earthquakes, the form of the source time function is somewhat different from that in cases 1 and 2.

5. Discussion and Conclusions

[49] To understand the loading processes of megathrust earthquakes along the Nankai subduction zone, it is necessary to model short-term SSEs because they occur along the immediately deeper extension of the fault zone from where such megathrust earthquakes occur. Based on the study

performed by *Shibazaki and Shimamoto* [2007], we developed a model of short-term SSEs on the 3-D subduction interface beneath Shikoku, southwest Japan, considering a rate- and state-dependent friction law with a small cutoff velocity for the evolution effect. In the case that the cutoff velocity for the evolution effect is considerably smaller than that for the direct effect, the steady state friction exhibits velocity weakening at low slip velocity and velocity strengthening at high slip velocity. We assume that pore pressure is nearly equal to lithostatic pressure and that critical displacement is very small within the generation zone of SSEs.

[50] By considering a 3-D plate interface, we can set the SSE zone appropriately, based on the hypocentral distribution of low-frequency tremors. We set three segments of SSEs: a larger segment beneath western Shikoku and two smaller segments beneath central and eastern Shikoku. This model is able to reproduce events beneath the western part of Shikoku with greater lengths in the along-strike direction and with longer recurrence times. The numerical results are consistent with the observation by *Obara* [2010] that events within larger segments have longer recurrence intervals. The stress loading rate in a large segment is lower than that in a small segment. Therefore, events that occur at the large segment have longer recurrence intervals and larger moment releases than those that occur at a small segment. The reproduced events propagate along strike at a speed of 5–50 km/d, consistent with the observation of
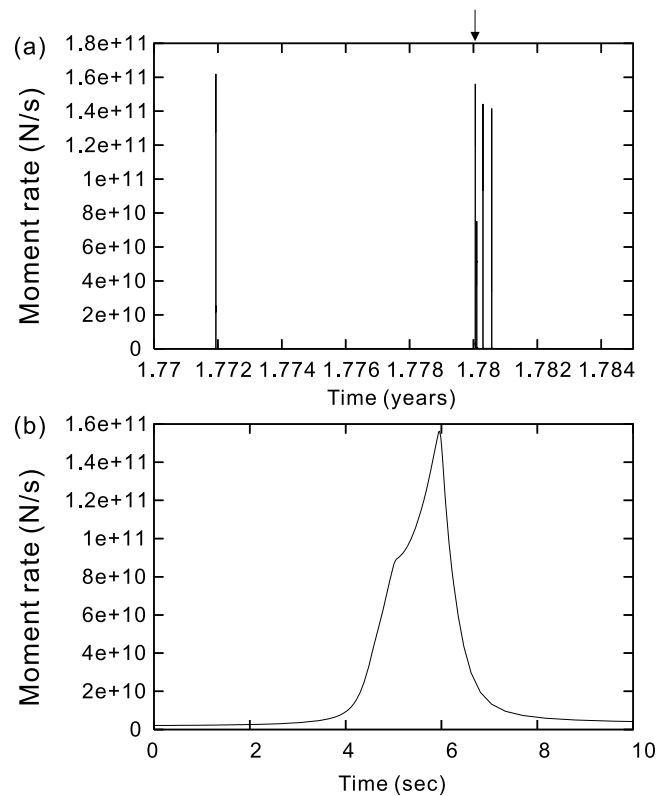
Figure 13. (a) Moment rate for a typical SSE on a 1-D fault in case 2. Several strong VLF events occur during a single SSE. (b) Moment rate with an extended time scale for the VLF event indicated by the arrow in Figure 13a.
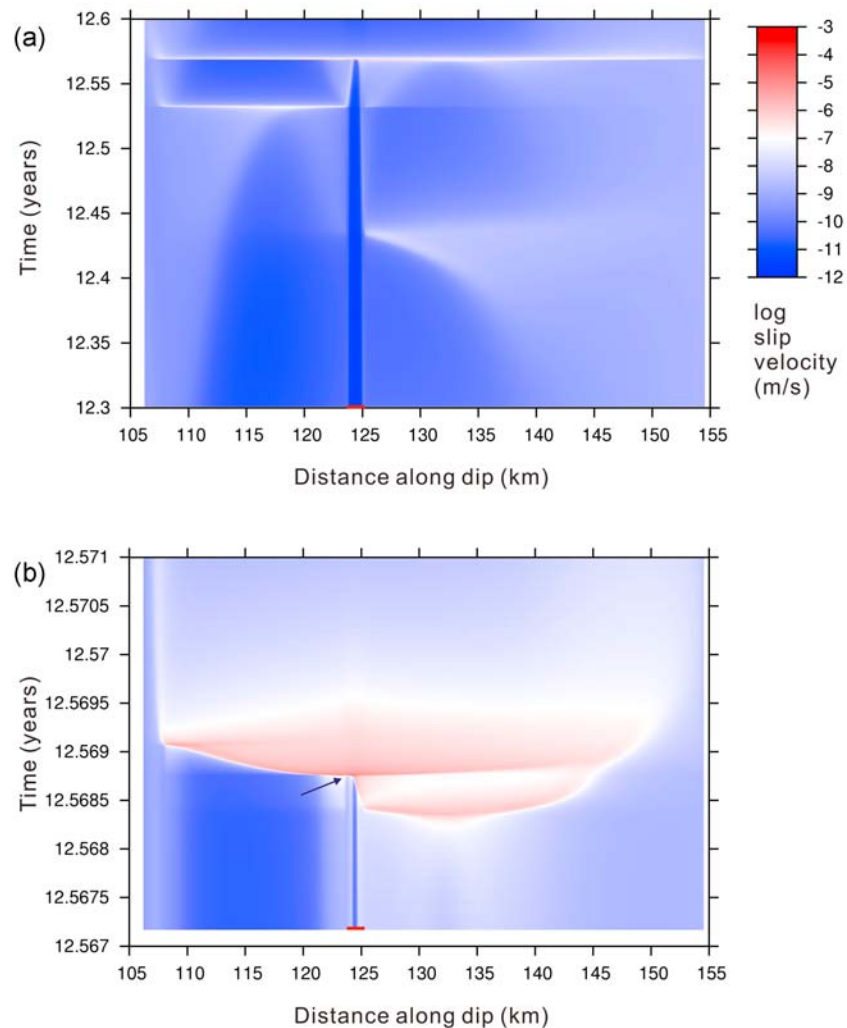
Figure 14. (a) Spatial distribution of slip velocity over time during 0.3 year in case 3. Three SSEs occur during this period. (b) Spatial distribution of slip velocity for the large SSE at t = 12.569 years. The red bars in Figures 14a and 14b indicate the location of the patch of VLF earthquakes.

Obara [2010] that the along-strike propagation speed of events ranges from approximately 5 to 20 km/d.

[51] Multisegment events are modeled in the western and central segments or central and eastern segments, along with rare three-segment events, consistent with observed SSEs. For an increased width of connection zone between segments, multisegment events occur more frequently and the style of SSE activity differs from that observed. It is concluded that the activity of SSEs is determined by nonuniform frictional properties within the transition zone.

[52] We also attempted to model the VLF earthquakes accompanied by short-term SSEs. To model such earthquakes, we considered a local patch in which the constitutive law parameters were varied. We considered three cases for reproducing VLF earthquakes. First, we assumed a smaller critical displacement for the patch. We can confirm that multiple slips occur at the patch during a single SSE; in addition, the moment rate for a single SSE shows a gradual increase and decrease. In this case, because of a small critical displacement, a drop in the frictional strength and healing

occur quickly at the local patch. The progress of an SSE increases stress at the local patch continuously. As a result, fast slip events occur repeatedly at the local patch.

[53] In modeling foreshocks with slow rupture growth during the nucleation process, *Shibazaki and Matsu'ura* [1995] considered a small patch with a relatively small critical displacement, located within a broad weak zone with a relatively large critical displacement. *Ide and Aochi* [2005] developed a model of the wide-scale growth of dynamic rupture during an earthquake assuming that critical displacement and fracture surface energy have multiscale heterogeneous distributions. There is a possibility that critical displacement scales with the size of events even at the deep subduction interfaces.

[54] Second, we assumed a larger cutoff velocity and a smaller critical displacement. This case produces an event with a fast rupture and small stress drop. The maximum moment rate is much larger than those of other cases. The source time function is simple: it rapidly increases and then decreases. The form of the source time function appears to
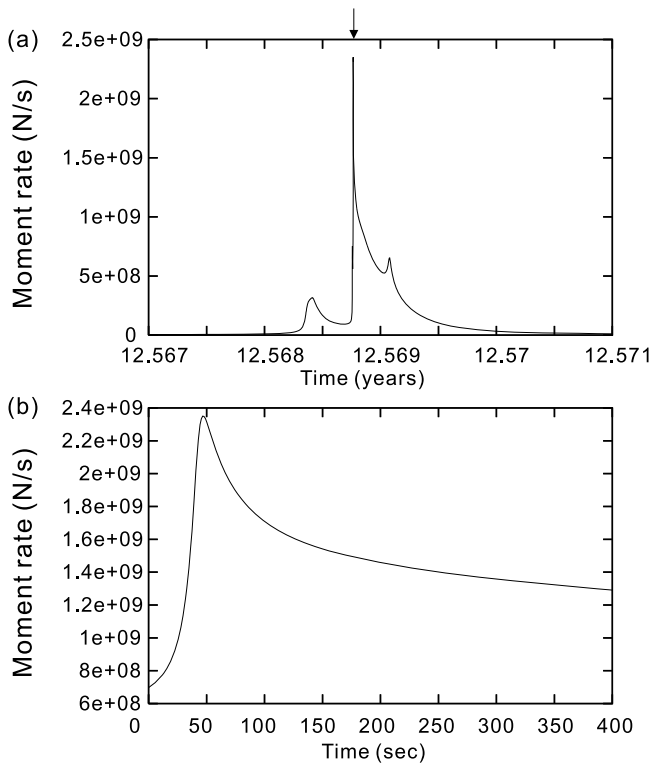
Figure 15. (a) Moment rate for the SSE on a 1-D fault in case 3, as shown in Figure 14b. (b) Moment rate with an extended time scale for the VLF event indicated by the arrow in Figure 15a and in Figure 14b.

be different from those observed [*Ide et al.*, 2008], which show a gradual increase and then decrease. Third, we considered the case in which the effective normal stress is 10 times that of the surrounding region. In this case, the patch acts as a barrier for some SSEs. When this barrier is ruptured, however, a larger SSE occurs. The source time function of the event has a sharp peak that corresponds to the rupture at the patch; the moment is subsequently released only slowly. Because the source time functions of the three cases are somewhat different, it will be possible to assess which is the appropriate model for VLF earthquakes by comparing the results with the observations. In the present study, we have considered only a 2-D fault model of VLF earthquakes. The source time functions of the 2-D fault model must be rather different from those of a 3-D fault model. Therefore, we need to construct a 3-D fault model of VLF earthquakes in the future.

[55] *Voisin et al.* [2008] investigated slip patterns using a laboratory friction experiment. They reproduced shallow earthquakes, slow events at medium depths, silent events at greater depths, and steady state creep at the greatest depth via aging of the contact interface with cumulative displacement. They also found that tremor-like signals are emitted by unstable slip at the contact asperity scale during silent slip events. A macroscopic SSE is possibly an aggregate of numerous small fast slip events (VLF earthquakes and LFTs). In our model, we simply made the constitutive law parameters in the area where VLF earthquakes occur different from those in the surrounding region. However, it will be

necessary to model numerous small fast slip events during the macroscopic SSE propagation.

[56] The present model does not consider fluid movement or changes in pore fluid pressure. *Segall and Rubin* [2007] succeeded in modeling SSEs while taking into account dilatancy-related changes in pore fluid pressure. It is possible that the behavior of pore fluid pressure controls the generation of SSEs. It also remains necessary to investigate the mechanism of pore pressure build-up at deeper levels of the subduction interface. We used a friction law with a small cutoff velocity for the evolution effect, with reference to the experiments by *Shimamoto* [1986], which were performed by progressively increasing the normal stress applied to halite at room temperature. Therefore, future studies should investigate the slip velocity dependence of the frictional properties in the unstable-stable transition regime with regard to several types of rocks under high-temperature conditions relevant to the depths at which short-term SSEs occur.

References

Beeler, N. (2009), Constructing constitutive relationships for seismic and aseismic fault slip, *Pure Appl. Geophys.*, *166*, 1775–1798, doi:10.1007/s00024-009-0523-0.

Ben-Zion, Y., and J. R. Rice (1997), Dynamic simulations of slip on a smooth fault in an elastic solid, *J. Geophys. Res.*, *102*(B8), 17,771–17,784, doi:10.1029/97JB01341.

Bréchet, Y., and Y. Estrin (1994), The effect of strain rate sensitivity on dynamic friction of metals, *Scr. Metall. Mater.*, *30*, 1449–1454, doi:10.1016/0956-716X(94)90244-5.

Dieterich, J. H. (1981), Constitutive properties of rock with simulated gouge, in *Mechanical Behavior of Crustal Rocks, Geophys. Monogr. Ser*, vol. 24, edited by N. L. Carter et al., pp. 108–120, AGU, Washington, D. C.

Dieterich, J. H. (1992), Earthquake nucleation on faults with rate- and state-dependent strength, *Tectonophysics*, *211*, 115–134, doi:10.1016/0040-1951(92)90055-B.

Dragert, H., K. Wang, and T. S. James (2001), A silent slip event on the deeper Cascadia subduction interface, *Science*, *292*, 1525–1528, doi:10.1126/science.1060152.

Dragert, H., K. Wang, and G. Rogers (2004), Geodetic and seismic signatures of episodic tremor and slip in the northern Cascadia subduction zone, *Earth Planets Space*, *56*, 1143–1150.

Estrin, Y., and Y. Bréchet (1996), On a model of frictional sliding, *Pure Appl. Geophys.*, *147*, 745–762, doi:10.1007/BF01089700.

Heki, K., and S. Miyazaki (2001), Plate convergence and long-term crustal deformation in central Japan, *Geophys. Res. Lett.*, *28*(12), 2313–2316, doi:10.1029/2000GL012537.

Hirose, H., and K. Hirahara (2004), A 3-D quasi-static model for a variety of slip behaviors on a subduction fault, *Pure Appl. Geophys.*, *161*, 2417–2431, doi:10.1007/s00024-004-2573-7.

Hirose, H., and K. Obara (2005), Repeating short- and long-term slow slip events with deep tremor activity around the Bungo channel region, southwest Japan, *Earth Planets Space*, *57*, 961–972.

Hirose, H., K. Hirahara, F. Kimata, N. Fujii, and S. Miyazaki (1999), A slow thrust slip event following the two 1996 Hyuganada earthquakes beneath the Bungo Channel, southwest Japan, *Geophys. Res. Lett.*, *26*(21), 3237–3240, doi:10.1029/1999GL010999.

Hori, T., N. Kato, K. Hirahara, T. Baba, and Y. Kaneda (2004), A numerical simulation of earthquake cycles along the Nankai Trough in southwest Japan: Lateral variation in frictional property due to the slab

geometry controls the nucleation position, *Earth Planet. Sci. Lett.*, *228*, 215–226, doi:10.1016/j.epsl.2004.09.033.

Ida, Y. (1973), The maximum acceleration of seismic ground motion, *Bull. Seismol. Soc. Am.*, *63*, 959–968.

Ide, S., and H. Aochi (2005), Earthquakes as multiscale dynamic ruptures with heterogeneous fracture surface energy, *J. Geophys. Res.*, *110*, B11303, doi:10.1029/2004JB003591.

Ide, S., G. C. Beroza, D. R. Shelly, and T. Uchide (2007), A scaling law for slow earthquakes, *Nature*, *447*, 76–79, doi:10.1038/nature05780.

Ide, S., K. Imanishi, Y. Yoshida, G. C. Beroza, and D. R. Shelly (2008), Bridging the gap between seismically and geodetically detected slow earthquakes, *Geophys. Res. Lett.*, *35*, L10305, doi:10.1029/2008GL034014.

Iio, Y., Y. Kobayashi, and T. Tada (2002), Large earthquakes initiate by the acceleration of slips on the downward extensions of seismogenic faults, *Earth Planet. Sci. Lett.*, *202*, 337–343, doi:10.1016/S0012-821X(02)00776-8.

Ito, Y., K. Obara, K. Shiomi, S. Sekine, and H. Hirose (2007), Slow earthquakes coincident with episodic tremors and slow slip events, *Science*, *315*, 503–506, doi:10.1126/science.1134454.

Kamaya, N., and A. Katsumata (2004), Low-frequency events away from volcanoes in the Japan islands, *J. Seismol. Soc. Jpn.*, *57*, 11–28.

Kato, N. (2003a), Repeating slip events at a circular asperity: Numerical simulation with a rate- and state-dependent friction law, *Bull. Earthquake Res. Inst. Univ. Tokyo*, *78*, 151–166.

Kato, N. (2003b), A possible model for large preseismic slip on a deeper extension of a seismic rupture plane, *Earth Planet. Sci. Lett.*, *216*, 17–25, doi:10.1016/S0012-821X(03)00483-7.

Kato, N., and T. Hirasawa (1997), A numerical study on seismic coupling along subduction zones using a laboratory-derived friction law, *Phys. Earth Planet. Inter.*, *102*, 51–68, doi:10.1016/S0031-9201(96)03264-5.

Kodaira, S., T. Iidaka, A. Kato, J. Park, T. Iwasaki, and Y. Kaneda (2004), High pore fluid pressure may cause silent slip in the Nankai trough, *Science*, *304*, 1295–1298, doi:10.1126/science.1096535.

Kuroki, H., H. M. Ito, H. Takayama, and A. Yoshida (2004), 3-D simulation of the occurrence of slow slip events in the Tokai region with a rate- and state-dependent friction law, *Bull. Seismol. Soc. Am.*, *94*, 2037–2050, doi:10.1785/0120030198.

Lapusta, N., and J. R. Rice (2003), Nucleation and early seismic propagation of small and large events in a crustal earthquake model, *J. Geophys. Res.*, *108*(B4), 2205, doi:10.1029/2001JB000793.

Linde, A. T., and I. S. Sacks (2002), Slow earthquakes and great earthquakes along the Nankai trough, *Earth Planet. Sci. Lett.*, *203*, 265–275, doi:10.1016/S0012-821X(02)00849-X.

Liu, Y., and J. R. Rice (2005), Aseismic slip transients emerge spontaneously in three-dimensional rate and state modeling of subduction earthquake sequences, *J. Geophys. Res.*, *110*, B08307, doi:10.1029/2004JB003424.

Liu, Y., and J. R. Rice (2007), Spontaneous and triggered aseismic deformation transients in a subduction fault model, *J. Geophys. Res.*, *112*, B09404, doi:10.1029/2007JB004930.

Marone, C. (1998), Laboratory-derived frictional laws and their application to seismic faulting, *Annu. Rev. Earth Planet. Sci.*, *26*, 643–696, doi:10.1146/annurev.earth.26.1.643.

Miller, M. M., T. Melbourne, D. J. Johnson, and W. Q. Sumner (2002), Periodic slow earthquakes from the Cascadia subduction zone, *Science*, *295*, 2423, doi:10.1126/science.1071193.

Mitsui, N., and K. Hirahara (2006), Slow slip events controlled by the slab dip and its lateral change along a trench, *Earth Planet. Sci. Lett.*, *245*, 344–358, doi:10.1016/j.epsl.2006.03.001.

Miyazaki, S., and K. Heki (2001), Crustal velocity field of southwest Japan: Subduction and arc-arc collision, *J. Geophys. Res.*, *106*(B3), 4305–4326, doi:10.1029/2000JB900312.

Miyazaki, S., P. Segall, J. J. McGuire, T. Kato, and Y. Hatanaka (2006), Spatial and temporal evolution of stress and slip rate during the 2000 Tokai slow earthquake, *J. Geophys. Res.*, *111*, B03409, doi:10.1029/2004JB003426.

Nakamura, M., H. Watanabe, T. Konomi, S. Kimura, and K. Miura (1997), Characteristic activities of subcrustal earthquakes along the outer zone of southwestern Japan, *Annu. Disaster Prev. Res. Inst. Kyoto Univ.*, *40*(B1), 1–20.

Nakata, R., N. Suda, and H. Tsuruoka (2008), Non-volcanic tremor resulting from the combined effect of Earth tides and slow slip events, *Nat. Geosci.*, *1*, 676–678, doi:10.1038/ngeo288.

Nakatani, M., and C. H. Scholz (2004a), Frictional healing of quartz gouge under hydrothermal conditions: 1. Experimental evidence for solution transfer healing mechanism, *J. Geophys. Res.*, *109*, B07201, doi:10.1029/2001JB001522.

Nakatani, M., and C. H. Scholz (2004b), Frictional healing of quartz gouge under hydrothermal conditions: 2. Quantitative interpretation with a physical model, *J. Geophys. Res.*, *109*, B07202, doi:10.1029/2003JB002938.

Obara, K. (2002), Nonvolcanic deep tremor associated with subduction in southwest Japan, *Science*, *296*, 1679–1681, doi:10.1126/science.1070378.

Obara, K. (2010), Phenomenology of deep slow earthquake family in southwest Japan: Spatiotemporal characteristics and segmentation, *J. Geophys. Res.*, doi:10.1029/2008JB006048, in press.

Obara, K., H. Hirose, F. Yamamizu, and K. Kasahara (2004), Episodic slow slip events accompanied by non-volcanic tremors in southwest Japan subduction zone, *Geophys. Res. Lett.*, *31*, L23602, doi:10.1029/2004GL020848.

Okubo, P. G. (1989), Dynamic rupture modeling with laboratory-derived constitutive relations, *J. Geophys. Res.*, *94*(B9), 12,321–12,335, doi:10.1029/JB094iB09p12321.

Ozawa, S., M. Murakami, and T. Tada (2001), Time-dependent inversion study of the slow thrust event in the Nankai trough subduction zone, southwestern Japan, *J. Geophys. Res.*, *106*(B1), 787–802, doi:10.1029/2000JB900317.

Ozawa, S., M. Murakami, M. Kaidzu, T. Tada, T. Sagiya, Y. Hatanaka, H. Yarai, and T. Nishimura (2002), Detection and monitoring of ongoing aseismic slip in the Tokai region, central Japan, *Science*, *298*, 1009–1012, doi:10.1126/science.1076780.

Press, W. H., S. A. Teukolsky, W. T. Vetterling, and B. P. Flannery (1992), *Numerical Recipes in Fortran: The Art of Scientific Computing*, 2nd ed., Cambridge Univ. Press, New York.

Rice, J. R. (1993), Spatio-temporal complexity of slip on a fault, *J. Geophys. Res.*, *98*(B6), 9885–9907, doi:10.1029/93JB00191.

Rogers, G. C., and H. Dragert (2003), Episodic tremor and slip on the Cascadia subduction zone: The chatter of silent slip, *Science*, *300*, 1942–1943, doi:10.1126/science.1084783.

Rubin, A. M., and J.-P. Ampuero (2005), Earthquake nucleation on (aging) rate and state faults, *J. Geophys. Res.*, *110*, B11312, doi:10.1029/2005JB003686.

Ruina, A. (1983), Slip instability and state variable friction laws, *J. Geophys. Res.*, *88*(B12), 10,359–10,370, doi:10.1029/JB088iB12p10359.

Sagiya, T., and W. Thatcher (1999), Coseismic slip resolution along a plate boundary megathrust: The Nankai Trough, southwest Japan, *J. Geophys. Res.*, *104*(B1), 1111–1129, doi:10.1029/98JB02644.

Segall, P. and A. Rubin (2007), Dilatancy stabilization of frictional sliding as a mechanism for slow slip events, *Eos Trans. AGU*, *88*(52), Fall Meet. Suppl., Abstract T13F-08.

Shelly, D. R., G. C. Beroza, S. Ide, and S. Nakamula (2006), Low-frequency earthquakes in Shikoku, Japan, and their relationship to episodic tremor and slip, *Nature*, *442*, 188–191, doi:10.1038/nature04931.

Shelly, D. R., G. C. Beroza, and S. Ide (2007), Complex evolution of transient slip derived from precise tremor locations in western Shikoku, Japan, *Geochem. Geophys. Geosyst.*, *8*, Q10014, doi:10.1029/2007GC001640.

Shibazaki, B., and Y. Iio (2003), On the physical mechanism of silent slip events along the deeper part of the seismogenic zone, *Geophys. Res. Lett.*, *30*(9), 1489, doi:10.1029/2003GL017047.

Shibazaki, B., and M. Matsu'ura (1995), Foreshocks and pre-events associated with the nucleation of large earthquakes, *Geophys. Res. Lett.*, *22*(10), 1305–1308, doi:10.1029/95GL01196.

Shibazaki, B., and T. Shimamoto (2007), Modelling of short-interval silent slip events in deeper subduction interfaces considering the frictional properties at the unstable-stable transition regime, *Geophys. J. Int.*, *171*, 191–205, doi:10.1111/j.1365-246X.2007.03434.x.

Shimamoto, T. (1986), Transition between frictional slip and ductile flow for halite shear zones at room temperature, *Science*, *231*, 711–714, doi:10.1126/science.231.4739.711.

Shimamoto, T. (1989), Mechanical behaviours of simulated halite shear zones: Implications for the seismicity along subducting plate-boundaries, in *Rheology of Solids and of the Earth*, edited by S. Karato and M. Toriumi, pp. 351–373, Oxford Univ. Press, Oxford, U. K.

Stuart, W. D., and T. E. Tullis (1995), Fault model for preseismic deformation at Parkfield, California, *J. Geophys. Res.*, *100*(B12), 24,079–24,099, doi:10.1029/95JB02517.

Stuart, W. D., T. Hildenbrand, and R. Simpson (1997), Stressing of the New Madrid Seismic Zone by a lower crust detachment fault, *J. Geophys. Res.*, *102*(B12), 27,623–27,633, doi:10.1029/97JB02716.

Tse, S. T., and J. R. Rice (1986), Crustal earthquake instability in relation to the depth variation of frictional slip properties, *J. Geophys. Res.*, *91*(B9), 9452–9472, doi:10.1029/JB091iB09p09452.

Voisin, C., J.-R. Grasso, E. Larose, and F. Renard (2008), Evolution of seismic signals and slip patterns along subduction zones: Insights from a friction lab scale experiment, *Geophys. Res. Lett.*, *35*, L08302, doi:10.1029/2008GL033356.

Yoshida, S., and N. Kato (2003), Episodic aseismic slip in a two-degree-of-freedom block-spring model, *Geophys. Res. Lett.*, *30*(13), 1681, doi:10.1029/2003GL017439.

Yoshioka, S., and K. Murakami (2007), Temperature distribution of the upper surface of the subducted Philippine Sea Plate along the Nankai Trough, southwest Japan, from a three-dimensional subduction model: Relation to large interplate and low-frequency earthquakes, *Geophys. J. Int.*, *171*, 302–315, doi:10.1111/j.1365-246X.2007.03510.x.

S. Bu, Department of Computer Science, University of Tsukuba, 1-1-1 Tennodai, Tsukuba, Ibaraki 305-8573, Japan.

H. Hirose and T. Matsuzawa, National Research Institute for Earth Science and Disaster Prevention, 3-1 Tennodai, Tsukuba, Ibaraki 305-0006, Japan.

B. Shibazaki, International Institute of Seismology and Earthquake Engineering, Building Research Institute, 1 Tatehara, Tsukuba 305-0802, Japan. (bshiba@kenken.go.jp)